Replicas of the Fano resonances induced by phonons in a subgap Andreev tunneling

J. Barański and T. Domański

Institute of Physics, M. Curie Skłodowska University, 20-031 Lublin, Poland
(Dated: January 17, 2013)

We study influence of the phonon modes on a subgap spectrum and Andreev conductance for the double quantum dot vertically coupled between a metallic and superconducting lead. For the monochromatic phonon reservoir we obtain replicas of the interferometric Fano-type structures appearing simultaneously in the particle and hole channels. We furthermore confront the induced on-dot pairing with the electron correlations and investigate how the phonon modes affect the zero-bias signature of the Kondo effect in Andreev conductance.

I.   INTRODUCTION

Electron transport through nano-size transistors containing the quantum dots, molecules and/or nanowires is determined by the available energy levels (tunable by external gate voltage) and strongly depends on the Coulomb interactions [1]. Discretization of the energy levels is responsible for oscillations of the differential conductance upon varying the gate voltage, whereas the correlation effects lead to the Coulomb blockade and can induce (at low temperatures) the Kondo resonance enhancing the zero-bias conductance to a unitary value $\frac{2e^2}{h}$ [2, 3]. Besides promising perspectives for the applications in modern electronics/spintronics the nanoscopic structures represent also valuable testing grounds for probing the many-body effects. Magnetic, superconducting or other types of orderings absorbed from the external leads can be confronted with the on-dot electron correlations in a fully controllable manner.

In this regard, especially interesting are the heterojunctions where the quantum dots (QDs) are in contact with the superconducting (S) electrodes. Nonequilibrium charge transport can occur there either via the usual single particle tunneling (upon breaking the electron pairs) or by activating the anomalous (Andreev or Josephson) channels. The resulting currents are sensitive to a competition between the induced on-dot pairing and the Coulomb repulsion. In such context there have been experimentally explored the signatures of π-junction [4], Josephson effect [5], superconducting quantum interference [6], quantum entanglement by splitting the Copper pairs [7], multiple Andreev scattering [8], and interplay of the on-dot pairing with the Kondo effect [9–11]. These and similar related activities have been discussed theoretically by various groups [12–16].

Since in practical realizations the nanoscopic objects are never entirely separated from an environment (e.g. a given substrate or external photon/phonon quanta) therefore transport properties are also affected by the interference effects. A convenient prototype for studying such phenomena is the tunneling setup shown in figure 1, where the central quantum dot is coupled to the side-attached quantum dot and eventually to other degrees of
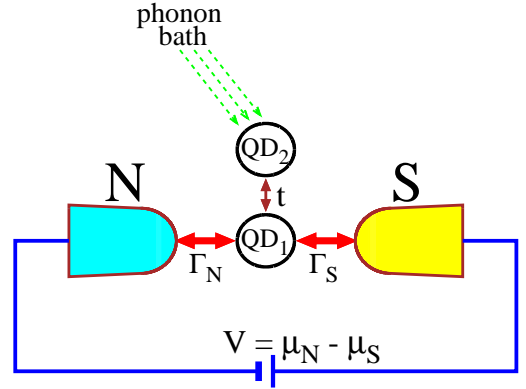

FIG. 1: (color online) Schematic view of the double quantum dot coupled in T-shape configuration between the metallic (N) and superconducting (S) electrodes where an external phonon bath affects the side-attached quantum dot (QD2).

freedom. Transport through this T-shape double quantum dot (DQD) occurs predominantly via the central quantum dot (QD$_1$), whereas electron leakage to/from the side-coupled quantum dot (QD$_2$) brings in the interference effects. In the case of both normal (N) electrodes and assuming a weak interdot coupling it has been argued [17, 18] that the differential conductance should reveal the asymmetric Fano-type lineshapes. This fact has been indeed observed experimentally [19].

Recently we have explored the interferometric patterns for the DQD case placed between the metallic and superconducting electrodes [20]. In such heterostructures the interferometric lineshapes appear simultaneously at negative and positive energies because of the mixed particle and hole degrees in the effective quantum dot spectrum [21]. These effects manifest themselves in the subgap Andreev conductance [10]. Stability of interferometric Fano structures on a dephasing by external fermionic bath have been analyzed in Refs [22, 23]. Here we extend such study addressing the role of bosonic bath in the setup displayed in Fig. 1. We argue that monochromatic phonon bath induces a number of the Fano-type replicas depending on the adiabadicity ratio λ/ω_0.

In the next section we introduce the microscopic model and briefly specify characteristic energy scales. We also discuss the formal aspects concerning the adopted approximations. In the section III we analyze spectroscopic fingerprints of the phonon modes for the case of uncorrected quantum dots. Finally, in section IV, we address the correlation effects (Coulomb blockade and Kondo physics) due to the on-dot repulsion between the opposite spin electrons. Appendix A provides phenomenological arguments for the Fano-type interferometric patters of the double quantum dot structures.

II. MICROSCOPIC MODEL

The double quantum dot heterojunction shown in Fig. 1 can be described by the Anderson-type Hamiltonian

$$\hat{H} = \hat{H}_{leads} + \hat{H}_{DQD} + \hat{H}_T \qquad (1)$$

where $\hat{H}_{leads} = \hat{H}_N + \hat{H}_S$ denote the normal N and superconducting S charge reservoirs, $\hat{H}_{DQD}$ refers to both quantum dots (together with the phonon bath) and the last term $\hat{H}_T$ describes the hybridization to external leads. We treat the conducting lead as a Fermi gas $\hat{H}_N = \sum_{\mathbf{k},\sigma} \xi_{\mathbf{k}N} \hat{c}^\dagger_{\mathbf{k}\sigma N} \hat{c}_{\mathbf{k}\sigma N}$ and we assume that isotropic superconductor is described by the BCS Hamiltonian $\hat{H}_S = \sum_{\mathbf{k},\sigma} \xi_{\mathbf{k}S} \hat{c}^\dagger_{\mathbf{k}\sigma S} \hat{c}_{\mathbf{k}\sigma S} - \Delta \sum_{\mathbf{k}} (\hat{c}^\dagger_{\mathbf{k}\uparrow S} \hat{c}^\dagger_{-\mathbf{k}\downarrow S} + \hat{c}_{-\mathbf{k}\downarrow S} \hat{c}_{\mathbf{k}\uparrow S})$. The operators $\hat{c}^{(\dagger)}_{\mathbf{k}\sigma\beta}$ correspond to annihilation (creation) of the itinerant electrons with spin $\sigma = \uparrow, \downarrow$ and energies $\xi_{\mathbf{k}\beta} = \varepsilon_{\mathbf{k}\beta} - \mu_\beta$ are measured with respect to the chemical potentials μ_β.

The double quantum dot along with the phonon bath is described by following local part

$$\hat{H}_{DQD} = \sum_{\sigma,i} \varepsilon_i \hat{d}^\dagger_{i\sigma} \hat{d}_{i\sigma} + t \sum_\sigma \left(\hat{d}^\dagger_{1\sigma} \hat{d}_{2\sigma} + \text{H.c.} \right) \qquad (2)$$
$$+ \sum_i U_i \, \hat{d}^\dagger_{i\uparrow} \hat{d}_{i\uparrow} \hat{d}^\dagger_{i\downarrow} \hat{d}_{i\downarrow} + \omega_0 \hat{a}^\dagger \hat{a} + \lambda \sum_\sigma \hat{d}^\dagger_{2\sigma} \hat{d}_{2\sigma} (\hat{a}^\dagger + \hat{a}),$$

where we use the standard notation for the annihilation (creation) operators $\hat{d}^{(\dagger)}_i$ for electrons at each quantum dot $QD_{i=1,2}$. Their energy levels are denoted by ε_i and U_i refer to the on-dot Coulomb potentials. Since we are interested in the Fano-type interference we focus on the electron transport only via the central quantum dot

$$\hat{H}_T = \sum_{\beta=N,S} \sum_{\mathbf{k},\sigma} \left(V_{\mathbf{k}\beta} \, \hat{d}^\dagger_{1\sigma} \hat{c}_{\mathbf{k}\sigma\beta} + \text{H.c.} \right). \qquad (3)$$

This situation can be extended to more general cases when electron tunneling directly involves both the quantum dots. For clarity reasons we postpone such analysis for the future studies.

A. Outline of the formalism

Energy spectrum and transport properties of the system (1) can be inferred from the matrix Green's function

$\boldsymbol{G}_i(\tau_1, \tau_2) = -i\hat{T}_\tau \langle \hat{\Psi}_i(\tau_1) \hat{\Psi}^\dagger_i(\tau_2) \rangle$ defined in a representation of the Nambu spinors $\hat{\Psi}^\dagger_i \equiv (\hat{d}^\dagger_{i\uparrow}, \hat{d}_{i\downarrow})$, $\hat{\Psi}_i \equiv (\hat{\Psi}^\dagger_i)^\dagger$. In the equilibrium conditions (for $\mu_N = \mu_S$) such matrix Green's function depends only on time difference $\tau_1 - \tau_2$. The corresponding Fourier transform can be then expressed by the Dyson equation

$$\boldsymbol{G}^{-1}_i(\omega) = \boldsymbol{g}^{-1}_i(\omega) - \boldsymbol{\Sigma}^0_i(\omega) - \boldsymbol{\Sigma}^U_i(\omega), \qquad (4)$$

where the bare propagators $\boldsymbol{g}_i(\omega)$ of uncorrelated quantum dots are given by

$$\boldsymbol{g}^{-1}_i(\omega) = \begin{pmatrix} \omega - \varepsilon_i & 0 \\ 0 & \omega + \varepsilon_i \end{pmatrix}. \qquad (5)$$

First part of the selfenergy $\boldsymbol{\Sigma}^0_i(\omega)$ comes from a combined effect of the interdot coupling, hybridization of the central QD_1 with the external leads (3) and the phonon bath contribution acting on QD_2. The other term $\boldsymbol{\Sigma}^U_i(\omega)$ appearing in (4) accounts for the many-body effects originating from the on-dot Coulomb repulsion U_i.

Let us begin by first specifying the selfenergy $\boldsymbol{\Sigma}^0_1(\omega)$ for the uncorrelated central quantum dot. The usual diagrammatic approach yields

$$\boldsymbol{\Sigma}^0_1(\omega) = \sum_{\mathbf{k},\beta} V_{\mathbf{k}\beta} \boldsymbol{g}_\beta(\mathbf{k}, \omega) V^*_{\mathbf{k}\beta} + t \, \boldsymbol{G}_2(\omega) \, t^*, \qquad (6)$$

where $\boldsymbol{g}_\beta(\mathbf{k}, \omega)$ denote the matrix Green's functions of the leads. In particular, we have for the normal lead

$$\boldsymbol{g}_N(\mathbf{k}, \omega) = \begin{pmatrix} \frac{1}{\omega - \xi_{\mathbf{k}N}} & 0 \\ 0 & \frac{1}{\omega + \xi_{\mathbf{k}N}} \end{pmatrix} \qquad (7)$$

and for the superconducting electrode

$$\boldsymbol{g}_S(\mathbf{k}, \omega) = \begin{pmatrix} \frac{u^2_{\mathbf{k}}}{\omega - E_{\mathbf{k}}} + \frac{v^2_{\mathbf{k}}}{\omega + E_{\mathbf{k}}} & \frac{-u_{\mathbf{k}} v_{\mathbf{k}}}{\omega - E_{\mathbf{k}}} + \frac{u_{\mathbf{k}} v_{\mathbf{k}}}{\omega + E_{\mathbf{k}}} \\ \frac{-u_{\mathbf{k}} v_{\mathbf{k}}}{\omega - E_{\mathbf{k}}} + \frac{u_{\mathbf{k}} v_{\mathbf{k}}}{\omega + E_{\mathbf{k}}} & \frac{u^2_{\mathbf{k}}}{\omega + E_{\mathbf{k}}} + \frac{v^2_{\mathbf{k}}}{\omega - E_{\mathbf{k}}} \end{pmatrix} \qquad (8)$$

with quasiparticle energy $E_{\mathbf{k}} = \sqrt{\xi^2_{\mathbf{k}S} + \Delta^2}$ and the BCS coefficients $u^2_{\mathbf{k}}, v^2_{\mathbf{k}} = \frac{1}{2} \left[1 \pm \frac{\xi_{\mathbf{k}S}}{E_{\mathbf{k}}} \right]$, $u_{\mathbf{k}} v_{\mathbf{k}} = \frac{\Delta}{2E_{\mathbf{k}}}$. In the wide band limit approximation we assume the constant hybridization couplings $\Gamma_\beta = 2\pi \sum_{\mathbf{k}} |V_{\mathbf{k}\beta}|^2 \delta(\omega - \xi_{\mathbf{k}\beta})$ and treat Γ_N as a convenient unit for energies. We then formally have

$$\sum_{\mathbf{k}} |V_{\mathbf{k}N}|^2 \, \boldsymbol{g}_\beta(\mathbf{k}, \omega) = -i\frac{\Gamma_N}{2} \begin{pmatrix} 1 & 0 \\ 0 & 1 \end{pmatrix} \qquad (9)$$

$$\sum_{\mathbf{k}} |V_{\mathbf{k}S}|^2 \, \boldsymbol{g}_S(\mathbf{k}, \omega) = -i\frac{\Gamma_S}{2} \gamma(\omega) \begin{pmatrix} 1 & \frac{\Delta}{\omega} \\ \frac{\Delta}{\omega} & 1 \end{pmatrix} \qquad (10)$$

where [12]

$$\gamma(\omega) = \begin{cases} \frac{|\omega|}{\sqrt{\omega^2 - \Delta^2}} & \text{for } |\omega| > \Delta, \\ \frac{\omega}{i\sqrt{\Delta^2 - \omega^2}} & \text{for } |\omega| < \Delta. \end{cases} \qquad (11)$$

Deep in a subgap regime (i.e. for $|\omega| \ll \Delta$) only the off-diagonal terms of (10) survive, approaching the static

value $-\Gamma_S/2$. From the physical point of view a magnitude $|-\Gamma_S/2| \equiv \Delta_{d1}$ can be interpreted as on-dot pairing gap induced in the QD$_1$. Such situation has been studied in the literature by a number of authors [24] applying various methods to account for the correlation effects $\Sigma_1^U(\omega)$.

B.   Influence of the phonon modes

Generally speaking, the phonon modes have both the quantitative and qualitative influence on the electron transport through nanodevices [25]. In particular they can be responsible for such effects as: appearance of the multiple side-peaks, polaronic shift in the energy levels, lowering of the on-dot potential U_i (even to the negative values promoting the pair hopping [26]), suppression of the hybridization couplings Γ_β and often serve as a source of the decoherence. These and related subjects have been so far studied by many groups, mainly considering the single quantum dots coupled to the normal leads [27]. Here we would like to focus on the different situation (Fig. 1) considering the phonon modes coupled to the side-attached quantum dot. This is reminiscent of the setup discussed by M. Büttiker [28] except that the fermion reservoir is here replaced by the phonon bath.

In analogy to (6) we express the selfenergy $\boldsymbol{\Sigma}_2^0(\omega)$ of QD$_2$ by the following contributions

$$\boldsymbol{\Sigma}_2^0(\omega) = t\boldsymbol{G}_1(\omega)t^* + \boldsymbol{\Sigma}_2^{ph}(\omega), \qquad (12)$$

where $t\boldsymbol{G}_1(\omega)t^*$ originates from the interdot hybridization and the second term is induced by the phonon reservoir. Since QD$_2$ is assumed to be weakly coupled with the central dot we approximate the selfenergy $\boldsymbol{\Sigma}_2^{ph}(\omega)$ adopting the local solution. The selfenergy $\boldsymbol{\Sigma}_2^{ph}(\omega)$ can be determined by means of the Lang-Firsov canonical transformation which effectively gives [29]

$$\frac{1}{\omega - \varepsilon_2 - \boldsymbol{\Sigma}_2^{ph}(\omega)} = \sum_l \begin{pmatrix} \frac{\mathcal{A}(l)}{\omega - \tilde{\varepsilon}_2(l)} & 0 \\ 0 & \frac{\mathcal{A}(l)}{\omega + \tilde{\varepsilon}_2(l)} \end{pmatrix} \qquad (13)$$

with the quasiparticle energies $\tilde{\varepsilon}_2(l) = \varepsilon_2 - \Delta_p + l\omega_0$, the corresponding polaronic shift $\Delta_p = \lambda^2/\omega_0$ and temperature dependent spectral weights $\mathcal{A}(l)$ [25, 29]

$$\mathcal{A}(l) = e^{-g\sqrt{1+2N_{ph}(l)}}\, e^{n\omega_0/k_BT} \qquad (14)$$
$$\times\ I_l\left(2g^2\sqrt{N_{ph}(l)\left[1+N_{ph}(l)\right]}\right).$$

As usually, we introduce a dimensionless adiabadicity parameter $g = \frac{\lambda^2}{\omega_0^2}$, $N_{ph}(l) = \left[e^{\omega_0/k_BT} - 1\right]^{-1}$ is the Bose-Einstein distribution and I_l denote the modified Bessel functions. In particular, for the ground state the equation (14) simplifies to

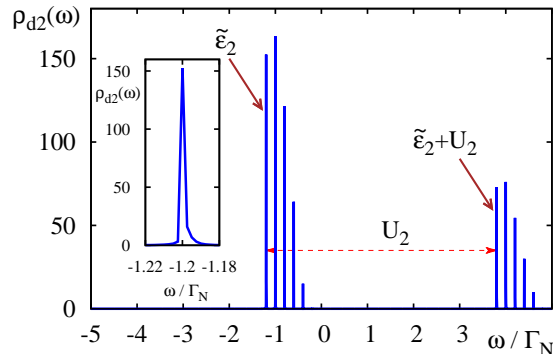$$\lim_{T \to 0} \mathcal{A}(l) = e^{-g}\frac{g^l}{l!}\,\theta(l). \qquad (15)$$

FIG. 2: (color online) Spectral function of the side-attached quantum dot obtained at low temperature for the model parameters $\varepsilon_2 = -1\Gamma_N$, $U_2 = 5\Gamma_N$, $\omega_0 = 0.2\Gamma_N$, $g = 1$, $\varepsilon_1 = 0$, $\Delta = 10\Gamma_N$ assuming a weak interdot coupling $t = 0.2\Gamma_N$.

In figure 2 we illustrate the characteristic spectrum of the side-attached quantum dot (see section IV.A for technical details). We notice two groups of the narrow peaks. The lower one starts from the energy $\tilde{\varepsilon}_2 = \varepsilon - \Delta_p$ (where $\Delta_p = \lambda^2/\omega_0$ is the polaronic shift) followed by a number of equidistant phonon peaks spaced by ω_0. The upper phonon branch is separated by U_2 and it manifests the charging effect [25]. For the coupling $g = 1$ we observe only about five phonon peaks but in the antiadiabatic regime ($g \gg 1$) their number considerably increases. Such tendency is shown in section III discussing the spectrum of QD$_1$. Let us also stress that the interference peaks have a rather tiny but yet finite width $\propto t^2/\Gamma_N$ [20].

C.   Subgap transport

Charge transport in a subgap regime $|eV| < \Delta$ is generated only by the Andreev mechanism. Electrons coming from the metallic lead are then converted into the Cooper pairs in superconductor simultaneously reflecting holes back to the normal lead. Such anomalous current $I_A(V)$ can be expressed by the Landauer-type formula [30]

$$I_A(V) = \frac{2e}{h}\int d\omega T_A(\omega)\left[f(\omega - eV, T) - f(\omega + eV, T)\right] \quad (16)$$

where $f(\omega, T) = 1/\left[e^{\omega/k_BT} + 1\right]$ is the Fermi-Dirac function. Andreev transmittance $T_A(\omega)$ depends on the off-diagonal part of the Green's function $\boldsymbol{G}_1(\omega)$ via [30]

$$T_A(\omega) = \Gamma_N^2\, |G_{1,12}(\omega)|^2. \qquad (17)$$

The transmittance (17) can be regarded as a qualitative measure of the proximity induced on-dot pairing. Under optimal conditions it approaches unity when ω is close to the quasiparticle energies $\pm\sqrt{\varepsilon_1^2 + (\Gamma_S/2)^2}$. The An-

dreev transmittance $T_A(\omega)$ is also sensitive to other structures, for instance originating from the interferometric effects [20, 22, 23].

In what follwos we shall study the differential Andreev conductance

$$G_A(V) = \frac{\partial I_A(V)}{\partial V} \qquad (18)$$

exploring its dependence on the phonon modes. We start this analysis assuming that both quantum dots uncorrelated and we next extend it (in section IV) by considering the correlation effects. As a general remark, let us notice that the even function $T_A(-\omega) = T_A(\omega)$ implies the symmetric Andreev conductance $G_A(-V) = G_A(V)$ regardless of any particular features due to interference, phonons, correlations or whatever. Physically this is caused by the fact that particle and hole degrees of freedom participate equally in the Andreev scattering.

III.   UNCORRELATED QUANTUM DOTS

Upon neglecting the correlation selfenergies $\Sigma_i^U(\omega) = 0$ one has to solve the following coupled equations

$$\boldsymbol{G}_1^{-1}(\omega) = \boldsymbol{g}_1^{-1}(\omega) - |t|^2 \boldsymbol{G}_2(\omega) + \frac{1}{2}\begin{pmatrix} i\Gamma_N & \Gamma_S \\ \Gamma_S & i\Gamma_N \end{pmatrix}(19)$$

$$\boldsymbol{G}_2^{-1}(\omega) = \boldsymbol{g}_2^{-1}(\omega) - |t|^2 \boldsymbol{G}_1(\omega) - \Sigma_2^{ph}(\omega). \qquad (20)$$

We have computed numerically the matrix Green's functions $\boldsymbol{G}_i(\omega)$ for a mesh of energy points appropriate for the model parameters (mainly dependent on ω_0, g and t). Practically already about ten iterations proved to yield a fairly convergent solution.

Since the proximity induced on-dot pairing predominantly affects the energy region around μ_S we first consider the instructive case $\varepsilon_1 = 0$, $\varepsilon_2 \neq \varepsilon_1$. In figure 3 we present the equilibrium spectrum $\rho_{d1}(\omega)$ of the central quantum dot obtained for three representative coupling constants $g = \lambda/\omega_0$ corresponding to the adiabatic limit $g \ll 1$ (upper panel), the antiadiabatic regime $g \gg 1$ (bottom panel) and the intermediate case (middle panel). On top of two Lorentzian peaks centered at the quasiparticle energies $\pm\Gamma_S/2$ we clearly see formation of the Fano resonances. They appear at energies $\tilde{\varepsilon}_2 + l\omega_0$ and at their mirror reflections (because of the particle - hole mixing [21]). Number of these phonon features depends on the adiabadicity parameter g. For the adiabatic regime there appear only a few phonon features whereas in the opposite antiadiabatic limit there is a whole bunch of such narrow structures. In the latter case they seem to have an irregular structure, but after closer inspection we can clearly see the Fano-type shapes (see the inset).

Phonon driven replicas of the Fano lineshapes appear also in the Andreev transmittance (see Fig. 4). In a distinction to the spectral function $\rho_{d1}(\omega)$ the resonances show up in a symmetrized way due to reasons mentioned
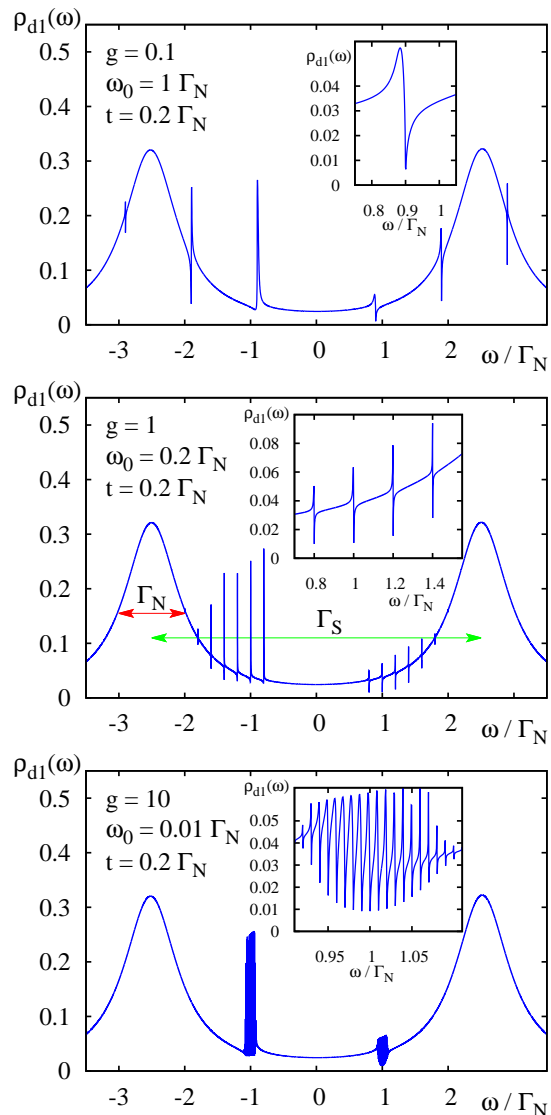

FIG. 3: (color online) The interferometric Fano-type lineshapes appearing at $T = 0$ in the spectral function $\rho_{d1}(\omega)$ of QD_1. Numerical calculations have been done for the uncorrelated quantum dots $U_i = 0$ using the model parameters $\varepsilon_1 = 0$, $\varepsilon_2 = 1\Gamma_N$, $t = 0.2\Gamma_N$, $\Gamma_S = 5\Gamma_N$ and $\Delta = 10\Gamma_N$.

in the preceding section. Again we notice the broad maxima centered at the subgap quasiparticle energies $\pm\Gamma_S/2$ accompanied by a number of the Fano-type resonances at $\pm(\tilde{\varepsilon}_2 + l\omega_0)$. Spectroscopic measurements of the Andreev conductance would thus be able to detect such phonon induced interferometric features.

The subgap quasiparticle lorentzian peaks (often referred as *the bound Andreev states*) depend on the energy level ε_1. In the case of single quantum dot (i.e. for vanishing t) the spectral function $\rho_{d1}(\omega)$ consists of two lorentzians at $\pm E_1$ (where $E_1 = \sqrt{\varepsilon_1^2 + (\Gamma_S/2)^2}$) broadened by Γ_N. Their spectral weights are given by
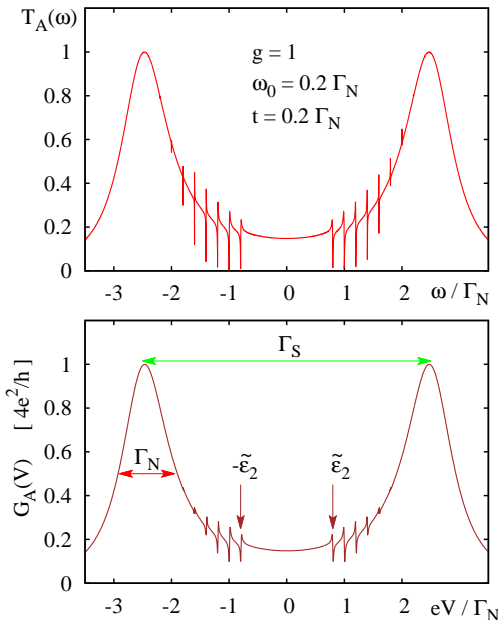
FIG. 4: (color online) The Andreev transmittance (upper panel) and the differential subgap conductance $G_A(V)$ (bottom panel) obtained for the intermediate coupling limit $g = 1$ using the same parameters as in figure 3.

the BCS factors $\frac{1}{2}(1 \pm \varepsilon_1/E_1)$. This fact has some importance also for the interferometric features. Figure 5 shows the spectrum $\rho_{d1}(\omega)$ for several values of ε_1. When the energy ε_1 moves away from the Fermi level (by applying the gate voltage) we observe a gradual redistribution of the quasiparticle spectral weights accompanied with suppression of the Fano resonances, especially at $-(\tilde{\varepsilon}_2 + l\omega_0)$. The Andreev transmittance $T_A(\omega)$ and differential conductance $G_A(V)$ are even functions therefore such particle-hole redistribution is not pronounced, nevertheless suppression of the phonon induced Fano lineshapes is well noticeable.

IV. CORRELATION EFFECTS

In this section we address qualitative effects caused by the Coulomb repulsion between the opposite spin electrons. Roughly speaking, we expect some possible signatures of the charging effect (Coulomb blockade) and eventual hallmarks of the Kondo physics. Since the electron transport occurs in our setup via QD_1 we suspect that predominantly the Coulomb potential U_1 can have a significant role. For completeness we shall however study the influence of correlations on both quantum dots.
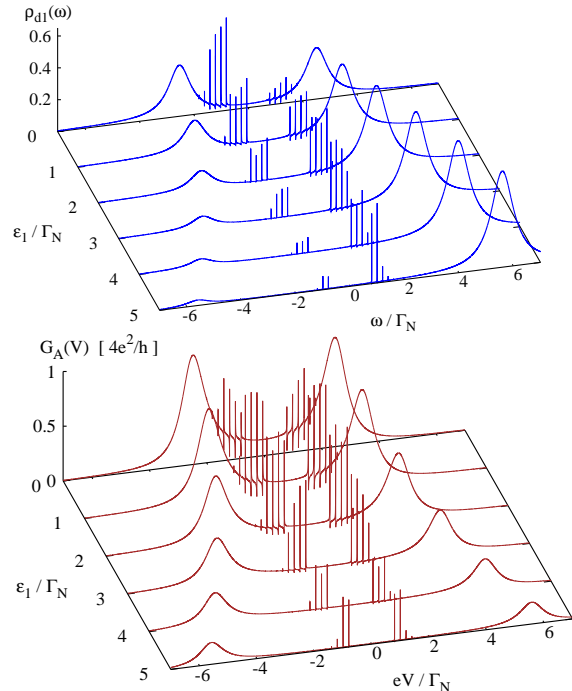

FIG. 5: (color online) Dependence of the spectral function $\rho_{d1}(\omega)$ and the Andreev conductance $G_A(V)$ on ε_1 (tunable by the gate voltage). Calculations have been done for the same parameters as in figure 4.

A. Influence of U_2

We start by considering the effects of finite U_2, neglecting correlations on the central quantum dot ($U_1 = 0$). Since the side-attached quantum dot is weakly hybridized with QD_1 therefore the indirect influence of external leads on QD_2 should be rather meaningless. For this reason we impose a diagonal structure of the selfenergy

$$\mathbf{\Sigma}_i^U(\omega) \simeq \begin{pmatrix} \Sigma_{i,\uparrow}^{diag}(\omega) & 0 \\ 0 & -\left[\Sigma_{i,\downarrow}^{diag}(-\omega)\right]^* \end{pmatrix}, \quad (21)$$

and here $i = 2$. We next approximate the diagonal terms of (21) by the atomic limit solution

$$\frac{1}{\omega - \varepsilon_2 - \Sigma_{2,\sigma}^{diag}(\omega)} = \frac{1 - n_{2,\bar{\sigma}}}{\omega - \varepsilon_2} + \frac{n_{2,\bar{\sigma}}}{\omega - \varepsilon_2 - U_2} \quad (22)$$

where $\bar{\downarrow} = \uparrow$, $\bar{\uparrow} = \downarrow$. It has been pointed out [31] that the selfenergy defined in equation (22) coincides with the second order perturbation formula

$$\Sigma_{2,\sigma}^{diag}(\omega) = U_2 n_{2,\bar{\sigma}} + \frac{(U_2)^2 n_{2,\bar{\sigma}}(1 - n_{2,\bar{\sigma}})}{\omega - \varepsilon_2 - U_2(1 - n_{2,\bar{\sigma}})} \quad (23)$$

and it can be generalized into more sophisticated treatments in the scheme of iterative perturbative theory [32].
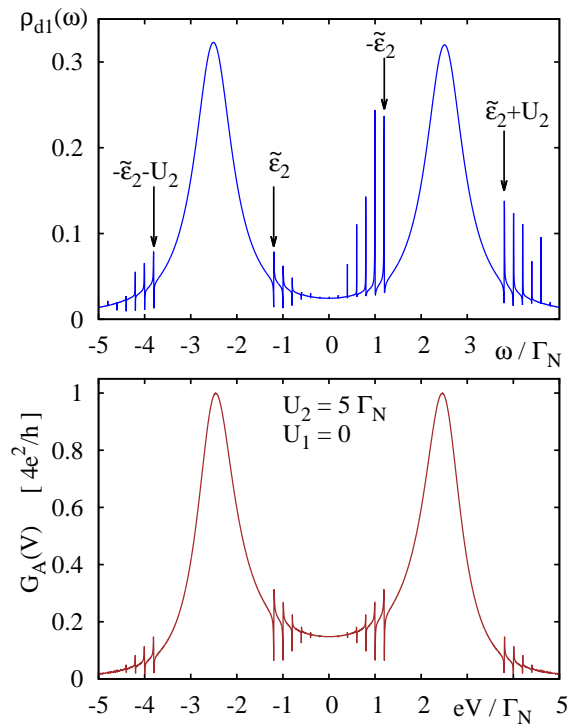
FIG. 6: (color online) Spectral function $\rho_{d1}(\omega)$ of the central quantum dot (top panel) and the differential Andreev conductance (bottom panel) obtained for $\varepsilon_1 = 0$, $\varepsilon_2 = -1\Gamma_N$, $t = 0.2\Gamma_N$, $g = 1$, $\omega_0 = 0.2\Gamma_N$, $\Delta = 10\Gamma_N$ assuming the Coulomb potential $U_2 = 5\Gamma_N$. The corresponding $\rho_{d2}(\omega)$ is shown in Fig. 2.

For the weak interdot coupling t we expect however that corrections to (22,23) are not crucial. We skip here the higher order superexchange mechanism leadind to the exotic Kondo effect [33] which is beyond the scope of our present study.

The top panel of figure 6 shows the spectrum $\rho_{d1}(\omega)$ obtained at low temperature for $U_2 = 5\Gamma_N$, $U_1 = 0$. As far as the side attached quantum dot spectrum is concerned it reveals a bunch of phonon peaks formed near the energy $\tilde{\varepsilon}_2$ and another group of states around the Coulomb satellite $\tilde{\varepsilon}_2 + U_2$ (see figure 2). These phonon signatures appear in $\rho_{d1}(\omega)$ as the Fano-type resonances. Due to the absorbed superconducting order we can notice effectively four groups of such Fano-type structures nearby the energies $\tilde{\varepsilon}_2$, $\tilde{\varepsilon}_2 + U_2$ and at their mirror reflections. The Andreev transmittance $T_A(\omega)$ is symmetrized versions of what is shown in figure 6 therefore the resulting differential conductance is even function of applied voltage V (see the bottom panel in Fig. 2).

B. Influence of U_1

Correlations originating from the Coulomb repulsion U_1 have a totally different effect on the transport prop-
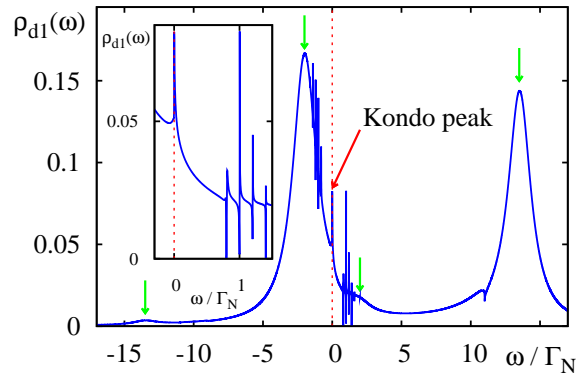

FIG. 7: (color online) Spectral function $\rho_{d1}(\omega)$ of the central quantum dot obtained in the Kondo regime for $k_B T = 10^{-3}\Gamma_N$, $\varepsilon_1 = -2\Gamma_N$, $U_2 = 15\Gamma_N$, $\Gamma_S = 4\Gamma_N$, $t = 0.2\Gamma_N$, $\omega_0 = 0.2\Gamma_N$, $g = 1$, $\Delta \gg \Gamma_N$. The vertical arrows indicate positions of the subgap Andreev states at $\pm E_1$ and at their Coulomb satellites. We can notice that the Kondo peak at $\omega = 0$ is distinct from the phonon induced Fano resonances.

erties than above discussed U_2. The central quantum dot is directly coupled to both external leads therefore on one hand by it experiences the induced on-dot pairing (due to Γ_S) and, the other hand, the Kondo effect (due to Γ_N). These phenomena are known to be antagonistic. Their nontrivial competition in a context of the quantum dots has been discussed theoretically by many groups using various techniques (see Ref. [13] for a survey).

To recover basic qualitative features we shall follow here our previous studies [34] which proved to yield satisfactory results for the single quantum dot on interface between the metallic and superconducting leads [10]. We choose the correlation selfenergy $\mathbf{\Sigma}_2^U(\omega)$ in the form (21) and determine its diagonal parts by the equation of motion approach [35]. Formally we use

$$\Sigma_{1,\sigma}^{diag}(\omega) = U_1 \left[n_{1,\bar{\sigma}} - \Sigma_1(\omega) \right] \qquad (24)$$
$$+ \frac{U_1 \left[n_{1,\bar{\sigma}} - \Sigma_1(\omega) \right] \left[\Sigma_3(\omega) + U_1(1 - n_{1,\bar{\sigma}}) \right]}{\omega - \varepsilon_1 - \Sigma_0(\omega) - \left[\Sigma_3(\omega) + U_1(1 - n_{1,\bar{\sigma}}) \right]},$$

where

$$\Sigma_\nu(\omega) = \sum_{\mathbf{k}} |V_{\mathbf{k}N}|^2 \left[\frac{1}{\omega - \xi_{\mathbf{k}N}} + \frac{1}{\omega - U_1 - 2\varepsilon_1 + \xi_{\mathbf{k}N}} \right]$$
$$\times \begin{cases} f(\xi_{\mathbf{k}N}) & \text{for } \nu = 1 \\ 1 & \text{for } \nu = 3 \end{cases} \qquad (25)$$

and as usually $\Sigma_0(\omega) = \sum_{\mathbf{k}} |V_{\mathbf{k}N}|^2/(\omega - \xi_{\mathbf{k}N}) = -i\Gamma_N/2$.

Let us remark that upon neglecting the terms $\Sigma_1(\omega)$ and $\Sigma_3(\omega)$ the selfenergy (24) nearly coincides with the second order perturbation formula (23)

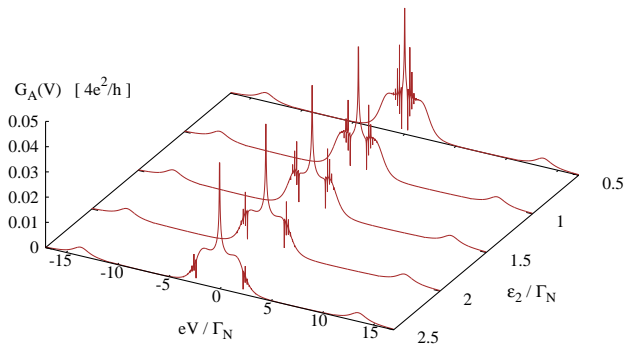$$\lim_{\Sigma_1, \Sigma_3 \to 0} \Sigma_{1,\sigma}^{diag}(\omega) = \qquad (26)$$

FIG. 8: (color online) The differential Andreev conductance $G_A(V)$ for the set of parameters discussed in figure 7 and several values of ε_2.

$$U_1 n_{1,\bar{\sigma}} + \frac{[U_1]^2 \, n_{1,\bar{\sigma}}(1-n_{1,\bar{\sigma}})}{\omega - \varepsilon_1 - U_1(1-n_{1,\bar{\sigma}}) - \Sigma_0(\omega)}$$

except of $\Sigma_0(\omega)$ present in the numerator of (27). This indicates that equation (24) is able to capture the charging effect (Coulomb blockade). The additional terms $\Sigma_\nu(\omega)$ provide corrections which are important in the Kondo regime, i.e. for $\varepsilon_1 < 0 < \varepsilon_1 + U_1$ at temperatures below $T_K = 0.29\sqrt{U_1\Gamma_N/2}\,\exp\left[\frac{\pi\varepsilon_1(\varepsilon_1+U_1)}{\Gamma_N U_1}\right]$. Under these conditions at μ_N there forms the narrow Kondo resonance of a width scaled by $k_B T_K$. In our present method such Kondo resonance is only qualitatively reproduced [34]. Its structure in the low energy regime $|\omega| \leq k_B T_K$ must be inferred from the renormalization group or other more sophisticated treatments.

Let us now point out the main properties characteristic for the Kondo regime. The equilibrium spectrum of QD_1 illustrated in figure 7 consists of four Andreev bound states (indicated by the vertical arrows) centered at $\pm\sqrt{\varepsilon_1^2 + (\Gamma_S/2)^2}$ and $\pm\sqrt{(\varepsilon_1 + U_1)^2 + (\Gamma_S/2)^2}$. The fact that ε_1 is located aside the superconducting energy gap causes asymmetry of the quasiparticle spectral weights. Besides these broad lorentzians we additionally notice the narrow peak at the Fermi level signifying the Kondo effect. Such Kondo peak is considerably reduced in comparison to the normal case $\Gamma_S = 0$ because of a competition with the on-dot pairing [34]. On top of this picture we recognize the phonon degrees of freedom appearing as the Fano-type resonances at $\pm(\tilde{\varepsilon}_2 + l\omega_0)$.

The above listed effects are also detectable in the differential Andreev conductance (see Fig. 8). $G_A(V)$ has local maxima at voltages corresponding to the energies of the subgap bound states. Furthermore, similarly to our previous studies [34], we notice that the Kondo peak leads enhances the zero-bias Andreev conductance. This property has been indeed observed experimentally [10]. In the present situation we additionally observe the Fano-type resonances. They destructively affect the zero-bias enhancement whenever the phonon features happen to be

located nearby the Kondo peak. The zero-bias feature itself is also quite sensitive to the asymmetry ratio Γ_S/Γ_N - practically it is visible only when both couplings Γ_β are comparable [34].

V. CONCLUSIONS

We have studied influence of the phonon modes on the spectral and on the Andreev transport in the double quantum dot vertically coupled between the metallic and superconducting electrodes. Our studies focused on the weak interdot coupling t assuming that phonons directly affect only the side-attached quantum dot. Under such circumstances an external phonon bath leads to some interferometric effects, reminiscent of the dephasing setup introduced by Büttiker [28].

In particular we find a number of the equidistant Fano-type patterns manifested both in the effective spectrum and in the subgap transport properties. These lineshapes appear at $\pm(\tilde{\varepsilon}_2 + l\omega_0)$ (where ω_0 is the phonon energy, l is an integer number and $\tilde{\varepsilon}_2 = \varepsilon_2 - \lambda^2/\omega_0$ describes the QD_2 energy shifted by a polaronic term). They can be regarded as *replicas* of the initial interferometric structures in absence of the phonon bath formed at $\pm\varepsilon_2$ [20, 23].

Electron correlations U_i on the quantum dots can induce additional Coulomb satellites of these Fano features. We have investigated in some detail how the correlation effects get along with the Fano interference taking into account the induced on-dot pairing. We notice that phonon features are sensitive to the subgap Andreev states (dependent on U_i) and to the Kondo effect. The latter one is important whenever the phonon lineshapes are induced in a vicinity of the Kondo peak. We thus expect that quantum interference would destructively affect the Kondo physics by partly suppressing its zero-bias hallmark [10].

It would be of interest for the future studies to check if the presently discussed effects are still preserved when the interdot coupling t is comparable to the external hybridization Γ_β. We suspect, that the Fano-type patterns shall evolve into some new qualities typical for the complex molecular structures. Furthermore, the role of Coulomb interaction U_2 might prove to be more influential via the higher order exchange integrations inducing some exotic kinds of the indirect Kondo effect [33]. These nontrivial issues deserve further studies eventually using some complementary methods.

Appendix A: Fano-type interference: phenomenological arguments

Here we would like to explain in a simple way why the interferometric Fano structures show up in the transport properties of DQD system. In general, the Fano-type lineshapes [36] emerge whenever the localized (resonant) electron waves interfere with a continuum (or with sufficiently broad electron states). Following [37] let us consider the very instructive example in which the "direct" transmission channel $t_d = \sqrt{G_d} e^{i\phi_d}$ (here G_d denotes its conductance and ϕ_d stands for an arbitrary phase) is combined with the transmission amplitude $t_r(\omega) = \sqrt{G_r} \frac{(\Gamma_L+\Gamma_R)/2}{\omega-\varepsilon_r+i(\Gamma_L+\Gamma_R)/2}$ of another "resonant" level ε_r. From general considerations [35] the corresponding conductance of such "resonant" level is $G_r = \frac{2e^2}{h} \frac{4\Gamma_L\Gamma_R}{(\Gamma_L+\Gamma_R)^2}$. Effectively these two channels yield the following asymmetric structure

$$G(\omega) = |t_d + t_r(\omega)|^2 = G_d \frac{|\tilde{\omega}+q|^2}{\tilde{\omega}^2+1}, \qquad (A1)$$

where $\tilde{\omega} = (\omega - \varepsilon_r)/(\frac{1}{2}\Gamma)$ and $q = i + e^{-i\phi_d}\sqrt{\frac{G_r}{G_d}}$ is the characteristic asymmetry factor.

Similar reasoning can be applied to the T-shape double quantum dot system shown in Fig. 1. For simplicity let as neglect the phonon bath and assume that both electrodes are normal conductors. In the case of weak interdot coupling $t^2 \ll \Gamma_\beta^2$ the side-attached dot QD$_2$ plays the role of "resonant" channel with its transmission amplitude $t_r(\omega) = \sqrt{G_r} \frac{t/2}{\omega-\varepsilon_2+it/2}$, where $G_r = \frac{2e^2}{h}$. On the other hand the other central dot QD$_1$ provides a relatively broad background $t_d(\omega) = \sqrt{\frac{2e^2}{h} \frac{4\Gamma_N\Gamma_S}{(\Gamma_N+\Gamma_S)^2}} \frac{(\Gamma_N+\Gamma_S)/2}{\omega-\varepsilon_1+i(\Gamma_N+\Gamma_S)/2}$. For energies $\omega \sim \varepsilon_2$ the latter amplitude is nearly constant $t_d(\omega) \simeq \sqrt{G_d}e^{i\phi_d}$ with $\sqrt{G_d} = \sqrt{\frac{2e^2}{h} \frac{4\Gamma_N\Gamma_S}{(\Gamma_N+\Gamma_S)^2}} \left| \frac{1}{2(\varepsilon_1-\varepsilon_2)/(\Gamma_N+\Gamma_S)+i} \right|$. Under such conditions the resulting conductance $G(\omega) = |t_d + t_r(\omega)|^2$ indeed reduces to the Fano structure (A1). Some more specific microscopic arguments in support for the Fano-type interference of the strongly correlated quantum dots have been discussed at length e.g. by Maruyama [17] and by Žitko [18].

[1] I.L. Aleiner, P.W. Brouwer, and L.I. Glazman, Phys. Rep. **358**, 309 (2002); M. Pustilnik and L.I. Glazman, J. Phys." Condens. Matter **16**, 513R (2004).

[2] D. Goldhaber-Gordon, J. Göres, M.A. Kastner, H. Shtrikman, D. Mahalu, and U. Meirav, Phys. Rev. Lett. **81**, 5225 (1998).

[3] W.G. van der Wiel, S. De Franceschi, T. Fujisawa, J.M. Elzerman, S. Tarucha, and L.P. Kouwenhoven, Science **289**, 2105 (2000); L.P. Kouwenhoven, D.G. Austing, and S. Tarucha, Rep. Prog. Phys. **64**, 701 (2001).

[4] J.A. van Dam, Y.V. Nazarov, E.P.A.M. Bakkers, S. De Franceschi, and L.P. Kouwenhoven, Nature (London) **442**, 667 (2006); H.I. Jorgensen, T. Novotny, K. Grove-Rasmussen, K. Flensberg, and P.E. Lindelof, Nano Lett. **7**, 2441 (2007).

[5] M.R. Buitelaar, T. Nussbaumer, and C. Schönenberger, Phys. Rev. Lett. **89**, 256801 (2002); P. Jarillo-Herrero, J.A. van Dam, and L.P. Kouwenhoven, Nature (London) **439**, 953 (2006); H.I. Jorgensen, K. Grove-Rasmussen, T. Novotny, K. Flensberg, and P.E. Lindelof, Phys. Rev. Lett. **96**, 207003 (2006).

[6] J.-P. Cleuziou, W. Wernsdorfer, V. Bouchiat, T. Ondarcuhu, and M. Monthioux, Nat. Nanotechnol. **1**, 53 (2006).

[7] L. Hofstetter, S. Csonka, J. Nygard, and C. Schönenberger, Nature (London) **461**, 960 (2009); L.G. Herrmann, F. Portier, P. Roche, A. Levy Yeyati, T. Kontos, and C. Strunk, Phys. Rev. Lett. **104**, 026801 (2010).

[8] M.R. Buitelaar, W. Belzig, T. Nussbaumer, B. Babić, C. Bruder, and C. Schönenberger, Phys. Rev. Lett. **91**, 057005 (2003); L. DellAnna, A. Zazunov, and R. Egger, Phys. Rev. B **77**, 104525 (2008).

[9] J.-D. Pillet, C.H.L. Quay, P. Morfin, C. Bena, A. Levy Yeyati, and P. Joyez, Nat. Phys. **6**, 965 (2010).

[10] R.S. Deacon, Y. Tanaka, A. Oiwa, R. Sakano, K. Yoshida, K. Shibata, K. Hirakawa, and S. Tarucha, Phys. Rev. Lett. **104**, 076805 (2010); R.S. Deacon, Y. Tanaka, A. Oiwa, R. Sakano, K. Yoshida, K. Shibata, K. Hirakawa, and S. Tarucha, Phys. Rev. B **81**, 121308(R) (2010).

[11] E.J.H. Lee, X. Jiang, R. Aguado, G. Katsaros, Ch.M. Lieber, and S. De Franceschi, Phys. Rev. Lett. **109**, 186802 (2012); S. De Franceschi, L.P. Kouwenhoven, C. Schönenberger, and W. Wernsdorfer, Nature Nanotechnol. **5**, 703 (2010).

[12] Y. Yamada, Y. Tanaka, and N. Kawakami, Phys. Rev. B **84**, 075484 (2011).

[13] A. Martín-Rodero and A. Levy Yeyati, Adv. Phys. **60**, 899 (2011).

[14] V. Koerting, B.M. Andersen, K. Flensberg, and J. Paaske, Phys. Rev. B **82**, 245108 (2010); A. Oguri, Y. Tanaka, and J. Bauer, arXiv:1210.3260 (preprint).

[15] S. Droste, S. Andergassen, and J. Splettstoesser, J. Phys.: Condens. Matter **24**, 415301 (2012).

[16] A.G. Moghaddam, M. Governale, and J. König, Phys. Rev. B **85**, 094518 (2012).

[17] I. Maruyama, N. Shibata, and K. Ueda, J. Phys. Soc. Jpn. **73**, 3239 (2004).

[18] R. Žitko, Phys. Rev. B **81**, 115316 (2010).

[19] S. Sasaki, H. Tamura, T. Akazaki, and T. Fujisawa, Phys. Rev. Lett. **103**, 266806 (2009).

[20] J. Barański and T. Domański, Phys. Rev. B **84**, 195424 (2011).

[21] A.V. Balatsky, I. Vekhter, and J.-X. Zhu, Rev. Mod. Phys. **78**, 373 (2006).

[22] J. Barański and T. Domański, Phys. Rev. B **85**, 205451 (2012).

[23] G. Michałek and B.R. Bułka, Acta Phys. Polon. A **122**, 981 (2012).

[24] Y. Tanaka, N. Kawakami, and A. Oguri, Phys. Rev. B **78**, 035444 (2008); *ibid* J. Phys.: Conf. Series **150**, 022086 (2009); T. Meng, S. Florens, and P. Simon, Phys. Rev. B 79, 224521 (2009); C. Karrasch, S. Andergassen, and V. Meden, Phys. Rev. B **84**, 134512 (2011).

[25] J. Fransson, *Non-Equilibrium Nano-Physics: A Many-Body Approach*, Lecture Notes in Physics **809** (Springer, Dordrecht 2010).

[26] J. Koch, M.E. Raikh, and F. von Oppen, Phys. Rev. Lett. **96**, 056803 (2006); K.I. Wysokiński, Phys. Rev. B **82**, 115423 (2010); S. Andergassen, T.A. Costi, and V. Zlatic, Phys. Rev. B **84**, 241107 (2011).

[27] J.-X. Zhu and A.V. Balatsky, Phys. Rev. B **67**, 165326 (2003); B. Dong, H.L. Cui, and X.L. Lei, Phys. Rev. B **69**, 205315 (2004); T. Novotny, A. Rossini, and K. Flensberg, Phys. Rev. B **72**, 224502 (2005); A. Ueda and M. Eto, Phys. Rev. B **73**, 235353 (2006); L. Siddiqui, A.W. Ghosh, and S. Datta, Phys. Rev. B **76**, 085433 (2007); T.-F. Fang, Q.-F. Sun, and H.-G. Luo, Phys. Rev. B **84**, 155417 (2011); G. Skorobagatko, Phys. Rev. B **85**, 075310 (2012); J. Ren, J.-X. Zhu, J.E. Gubernatis, C. Wang, and B. Li, Phys. Rev. B **85**, 155443 (2012); B.H. Wu, J.C. Cao, and C. Timm, Phys. Rev. B **86**, 035406 (2012).

[28] M. Büttiker, IBM J. Res. Develop. **32**, 63 (1998); M. Büttiker, Phys. Rev. Lett. **57**, 1761 (1986); M. Büttiker

[29] and C.A. Stafford, Phys. Rev. Lett. **76**, 495 (1996).

[29] G.D. Mahan, *Many-Particle Physics* (Plenum Press, New York, 1990).

[30] M. Krawiec and K.I. Wysokiński, Supercond. Sci. Technol. **17**, 103 (2004); Q.-F. Sun, H. Guo, and T.-H. Lin, Phys. Rev. Lett. **87**, 176601 (2001); Q.-F. Sun, J. Wang, and T.-H. Lin, Phys. Rev. B **59**, 3831 (1999).

[31] J.C. Cuevas, A. Levy Yeyati, and A. Martín-Rodero, Phys. Rev. B **63**, 094515 (2001).

[32] H. Kajueter and G. Kotliar, Phys. Rev. Lett. **77**, 131 (1996); A.A. Aligia, Phys. Rev. B **74**, 155125 (2006); A. Martín-Rodero, A. Levy Yeyati, F. Flores, and R.C. Monreal, Phys. Rev. B **78**, 235112 (2008); G. Górski and J. Mizia, arXiv:1211.6038 (preprint).

[33] Y. Tanaka, N. Kawakami, and A. Oguri, Phys. Rev. B **85**, 155314 (2012).

[34] T. Domański and A. Donabidowicz, Phys. Rev. B **78**, 073105 (2008); T. Domański, A. Donabidowicz, and K.I. Wysokiński, Phys. Rev. B **78**, 144515 (2008); Phys. Rev. B **76**, 104514 (2007).

[35] H. Haug and A.-P. Jauho, *Quantum Kinetics in Transport and Optics of Semiconductors*, (Springer, Berlin 2008).

[36] J. Göres, D. Goldhaber-Gordon, S. Heemeyer, M.A. Kastner, H. Shtrikman, D. Mahalu, and U. Meirav, Phys. Rev. B **62**, 2188 (2000).

[37] A.A. Clerk, X. Waintal, and P.W. Brouwer, Phys. Rev. Lett. **86**, 4636 (2001).